A numerical analysis of structural damage detection using changes in the curvature of power spectral density

パワースペクトル密度曲線の変化を用いた構造欠陥検出の数値解析

Sherif Beskhyroun*, Toshiyuki Oshima**, Shuichi Mikami*** and Tomoyuki Yamazaki****
シェリフ　ベスキロウン*, 大島俊之**, 三上修一***, 山崎智之****

*Doctoral Student, Dept. of Civil Eng., Kitami Institute of Technology, (165 Koen-cho, Kitami, 090-8507, Japan)
**Professor, Dept. of Civil Eng., Kitami Institute of Technology, (165 Koen-cho, Kitami, 090-8507, Japan)
***Associate Professor, Dept. of Civil Eng., Kitami Institute of Technology, (165 Koen-cho, Kitami, 090-8507, Japan)
****Research Associate, Dept. of Civil Eng., Kitami Institute of Technology, (165 Koen-cho, Kitami, 090-8507, Japan)

A change of modal characteristics can indicate structural damage. Based on changes in Power Spectral Density (PSD), this paper proposes a damage identification technique that detects damage and its location. The method is applied to a finite element model of a three span steel bridge with a concrete deck. Several damage scenarios were introduced to a main girder of the bridge. The method determined the exact damage location. In addition, the results illustrate that changes in the PSD curvature can be a useful tool for continuous monitoring of structural integrity using ambient vibration data. Furthermore, changes in the PSD curvature do not require a very fine grid of measurements to detect and locate damage effectively.
Key Words: vibration characteristics, damage detection, modal properties, health monitoring

1. Introduction

Recent natural disasters have amply demonstrated the need for rapid assessment of the performance and safety of civil structures such as bridges, control centers, airports, hospitals, and so forth. In addition, continuous loading and extreme environmental conditions have extensively deteriorated our infrastructure. The ability to monitor the structural integrity of these systems is becoming increasingly important. During the past two decades, numerous studies have addressed non-destructive damage evaluation (NDDE) via changes in the dynamic modal responses of a structure. All NDDE methods developed to date are classifiable into four levels according to their performance: [1,2)]

1. Level I – those methods that identify only whether damage has occurred.
2. Level II – those methods that identify whether damage has occurred and simultaneously determine the damage location.
3. Level III – those methods that identify whether damage has occurred, simultaneously determine the damage location, and further estimate the damage severity.
4. Level IV – those methods that identify if damage has occurred, simultaneously determine the damage location, estimate the damage severity, and assess the effect of that damage on the structure.

The level II non-destructive damage evaluation technique is performed in this study. Modal vibration data such as structural natural frequencies and mode shapes can characterize the state of the structure[3,4)]. This capability is attributable to the fact that damage in the form of changes in the structural physical properties (i.e., stiffness, mass, and boundary conditions) consequently alters such vibration properties of the structure as modal frequencies, mode shapes, and modal damping values[5)]. Changes in the vibration properties can then serve as indicators of damage detection. Techniques for detecting damage in a structure by monitoring these changes have attracted much attention in recent years; numerous approaches have been developed[6,7)].

The present paper describes a practical method to detect damage and locate its position using changes in the PSD curvature. First, we outline a damage detection algorithm to detect and locate damages in structures using changes in the PSD curvature. Next, we describe a numerical model for a three-span steel bridge, use the proposed

algorithm and the collected data to detect damages, and locate their positions in the test structure. Finally, we assess the practicality of the proposed algorithm by quantifying the accuracy of the obtained results from the test structure and comparing the respective performances of this algorithm and the previously reported method.

2. Proposed method's idea and theoretical description

Mode shapes and resonant frequencies are usually determined using conventional Frequency Response Function (FRF) spectral analysis techniques, which require measurement of the forcing function. For continuous health monitoring of structures, ambient vibrations are used as an excitation force. For example, traffic, wind, water waves, seismic ground motions or other environmental factors may cause ambient vibrations in bridges. One difficulty with determining dynamic parameters of a structure undergoing ambient vibrations is that the forcing function is not characterized precisely. McLamore et al.[8] introduced another technique for measuring modal data without measuring the excitation force. That study measured the motion of a bridge at different positions. Then the PSD for the motion response was used to estimate resonant frequencies. Mode shapes were estimated using the cross spectral density (CSD) between respective measuring channels and one reference channel[9]. In the proposed algorithm, the magnitude of PSD at all frequency components on the measurement range is used instead of using modal amplitude, which can be called operational mode shapes. Therefore, a small range of measurement can be used without the need for measuring modal data or higher modes. Moreover, PSD is calculated from the acceleration response without the need for measuring the excitation force.

2.1 Definition of Power Spectral Density

For a continuous time series, $x(t)$, defined on the interval from 0 to T, the Fourier Spectrum (Fourier Transform), $X(f)$, is defined as[9]

$$X(f) = \int_0^T x(t) e^{-i2\pi ft} dt \tag{1}$$

where $i = \sqrt{-1}$, and

f= cyclic frequency (Hz).

This function is complex. Its magnitude is typically plotted in engineering units (EU), such as m/s^2 or g, versus frequency. The power spectrum is defined as

$$|X(f)|^2 = X(f)X^*(f) \tag{2}$$

where * denotes a complex conjugate. The power spectrum is a real-valued frequency domain function with units of (EU)^2. The PSD, $G_x(f)$ is defined as

$$G_x(f) = \frac{2}{T} E\left[|X(f)|^2\right] \tag{3}$$

where $E[\ ]$ indicates an ensemble average for a specific f over n samples of $X(f)$. Again, this is a real-valued frequency domain function and has the units of (EU)^2/ Hz.

2.2 Proposed algorithm

Denote $G_i(f)$ the PSD magnitude measured at channel number i at frequency value f. Then $\{G(f)\}$ is a vector representing PSD magnitudes measured at all channels at the same frequency, f. Before analyzing PSD data, the PSD data must first be normalized. Several approaches can be used to normalize the PSD data. In this study, the approach taken was to normalize the PSD magnitudes at each frequency with respect to the square root of the sum of squares (SRSS), as shown in the following expression.

$$\{P(f)\} = \frac{1}{\sqrt{\sum_{i=1}^{n} G_i^2(f)}} \{G(f)\} \tag{4}$$

Therein, $\{P(f)\}$ represents the normalized PSD magnitudes, $\{G(f)\}$ designates the original PSD magnitudes at frequency f gathered experimentally or analytically, n is the number of measured points, and $G_i(f)$ is the PSD magnitude measured at channel i at frequency f. A polynomial can be fit to the PSD magnitudes and then subsequently differentiated to obtain curvature values. Interpolation of PSD data is explained in greater detail in section 3.1. The damage index is defined as the absolute difference in PSD curvature before and after damage as

$$S_i(f) = \left| P_i''(f) - P_i^{*''}(f) \right| \tag{5}$$

where $P_i''(f)$ and $P_i^{*''}(f)$ are the second derivative of PSD magnitude at frequency f at node i, corresponding respectively to an undamaged and damaged structure. Assuming that the collection of damage indices, $S_i(f)$, represents a sample population of a normally distributed random variable, a normalized damage indicator is obtained as

$$Q_i(f) = \frac{S_i(f) - \bar{S}(f)}{\sigma(f)} \tag{6}$$

where $\bar{S}(f)$ and $\sigma(f)$ represent the mean and standard deviation of the damage indices, respectively, and are defined as

$$\bar{S}(f) = \sum_{i=1}^{n} S_i(f) \Big/ n \tag{7}$$

$$\sigma(f) = \sqrt{\sum_{i=1}^{n} (S_i(f) - \bar{S}(f))^2} \Big/ (n-1) \tag{8}$$

The values of the normalized damage indicator (Eq. 6) measured at different points at the same frequency represent a vector $\{Q(f)\}$. When $Q_i(f)$ is calculated at different frequencies on the measurement range, from f_1 to f_m, then $[Q]$ is a matrix containing all values at different points and at different frequencies.

$$Q = \begin{bmatrix} Q_1(f_1) Q_1(f_2) \ldots\ldots Q_1(f_m) \\ Q_2(f_1) Q_2(f_2) \ldots\ldots Q_2(f_m) \\ . \\ . \\ Q_n(f_1) Q_n(f_2) \ldots\ldots Q_n(f_m) \end{bmatrix} \tag{9}$$

Therein, Q_{max} is the maximum absolute value of $[Q]$. In Eq. (5), it is

assumed that PSD curvature will change markedly at the damaged locations and slightly near the damaged zone (undamaged locations). Therefore, it is expected that $Q_i(f)$ will have bigger values at the damaged locations and smaller values at the undamaged locations. The sum of these small values of $Q_i(f)$ at the undamaged locations may degrade the actual position of damage and create false positive readings. Therefore, to reduce the effects of false positive readings, we must define a threshold before adding the value of the damage indicator over the different frequencies. A statistical decision-making procedure is employed to determine if the normalized damage index, $Q_i(f)$, is associated with a damage location. Different scenarios of damage (different sizes and different locations) were introduced to the numerical model. Using a value of 80% of Q_{max} as a limit to identify the damage location yields the best results. Using values less than 80% of Q_{max} will increase the possibility of false positive readings. Values greater than 80% of Q_{max} will reduce the ability to detect slight damage. To reduce the effect of positive false readings, $Q_i(f)$ values less than 80% of Q_{max} are removed and values greater than or equal to 80% of Q_{max} are added over different frequencies on the measurement range from f_1 to f_m. In other words,

if $|Q_i(f)| < (0.80 * Q_{max})$ then let $Q_i(f) = 0$ and $D_i(f) = 0$ (10)

if $|Q_i(f)| \geq (0.80 * Q_{max})$ then let $Q_i(f) = Q_i(f)$ and $D_i(f) = 1$ (11)

$$A_i = \sum_{f=f_1}^{f_m} |Q_i(f)| \tag{12}$$

In Eqs. (10) and (11), $D_i(f)$ is used as a counter to identify the number of times of detecting damage at node i. Adding the value of $D_i(f)$ over different frequencies gives the total number of times of detecting damage at node i on the measurement range as

$$O_i = \sum_{f=f_1}^{f_m} D_i(f) \tag{13}$$

Multiplying the damage index A_i by the total number of times O_i defines the accumulated damage indicator DI_i

$$DI_i = A_i O_i \tag{14}$$

2.3 Change in Cross Spectral Density Method

Change in CSD method[10] is based on changes, caused by damage, in strain energy stored in structural elements. The damage index is calculated using the magnitude of CSD as

$$\alpha_{f,j} = \frac{(\int_a^b [\phi_f^{*''}(x)]^2 dx + \int_0^L [\phi_f^{*''}(x)]^2 dx) \int_0^L [\phi_f''(x)]^2 dx}{(\int_a^b [\phi_f''(x)]^2 dx + \int_0^L [\phi_f''(x)]^2 dx) \int_0^L [\phi_f^{*''}(x)]^2 dx} \tag{15}$$

where $\phi_f''(x)$ and $\phi_f^{*''}(x)$ are the second derivatives of CSD magnitude at frequency f corresponding to the undamaged and damaged structure, respectively. L is beam length and a, b are the limits for element j. Assuming that the collection of the damage indices, $\alpha_{f,j}$, represents a sample population of a normally distributed random variable, a normalized damage indicator is obtained as

$$\lambda_{f,j} = \frac{\alpha_{f,j} - \overline{\alpha_f}}{\sigma_f} \tag{16}$$

where $\overline{\alpha_f}$ and σ_f represent the mean and standard deviation of the damage indices, respectively. A statistical decision-making procedure is employed to determine if the normalized damage index, λ_{fj}, is associated with a damage location. Values of four standard deviations from the mean are assumed to indicate damage locations. Therefore, to reduce the effect of false positive readings, $\lambda_{f,j}$ values less than four are removed and values greater than or equal to four are added over different frequencies on the measurement range, as shown in the following expressions.

if $|\lambda_{f,j}| < 4$, then let $\lambda_{f,j} = 0$ and $\kappa_{f,j} = 0$ (17)

if $|\lambda_{f,j}| \geq 4$, then let $\lambda_{f,j} = \lambda_{f,j}$ and $\kappa_{f,j} = 1$ (18)

When the normalized damage index, λ_{fj}, is calculated using the magnitude of CSD at different frequencies on the measurement range from *F1 to F2*, the new damage index is defined as the sum of absolute values of damage indices measured at different frequencies.

$$\chi_j = \sum_{f=F1}^{F2} |\lambda_{f,j}| \tag{19}$$

In Eqs. (17) and (18), $\kappa_{f,j}$ is used as a counter to identify the number of times that damage is detected at element j. The sum of $\kappa_{f,j}$ over the different frequencies on the measurement range indicates the number of times of detecting damage at element j as the following.

$$\varepsilon_j = \sum_{f=F1}^{F2} \kappa_{f,j} \tag{20}$$

The product of damage index, χ_j, and the total number of times ε_j, defines Δ_j, the accumulated damage indicator.

$$\Delta_j = \chi_j \varepsilon_j \tag{21}$$

3. Numerical model

3.1 Description of the bridge finite element model

The bridge consists of three spans – the mid-span is 60 m, the outer spans are 40 m each – and the bridge width is 12 m. A finite element model of the bridge is shown in Fig. 1. Two steel plate girders and three steel stringers support the concrete deck. Loads from the stringers are transferred to the plate girders by floor beams located at 5 m intervals. Fig. 2 shows a cross section of the bridge. The numerical model of the bridge was created using the Structural Analysis Program SAP2000[11]. Shell elements represent the concrete deck, main girders, floor beams, and stringers. The FE model contains 7946 shell elements and 48030 active degrees of freedom (d.o.f.). The respective densities of steel and concrete are assumed as 77 and 24.5 kN/m^3. The moduli of elasticity of steel and concrete are assumed respectively as 206 and 25 GPa. The shaker excitation is

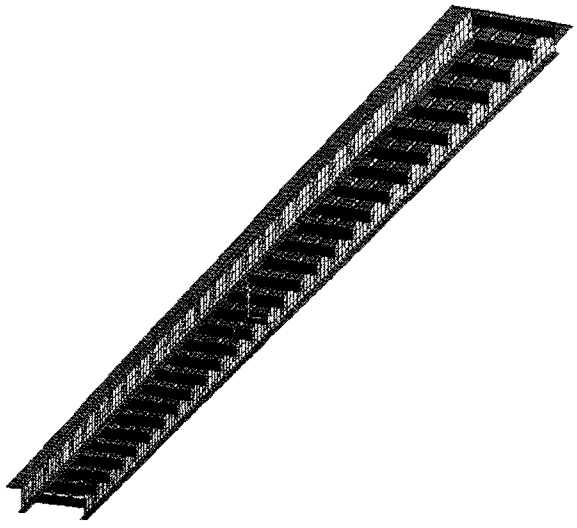

Fig. 1 Bridge model

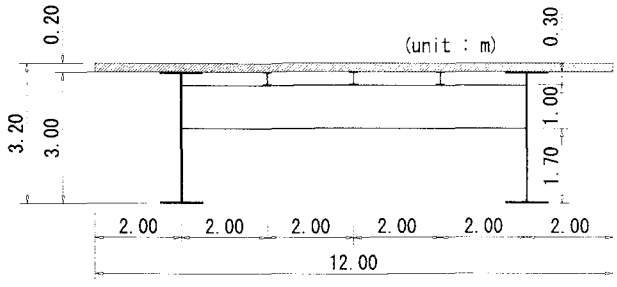

Fig. 2 Bridge cross section

simulated by a random time history signal with 4.90 kN peak amplitude. The random signal was defined by 1024 data points at 0.02 s increments. The excitation force is applied as a time-variant concentrated vertical load on the center of the bridge deck. Acceleration response in the vertical direction is measured at 21 nodes on the mid-span of the main girder, as shown in Fig. 3. Measuring points are located 1 m above the lower flange and spaced at 3 m (Fig. 3). The PSD is calculated from node point accelerations using MATLAB[12,13] standard and the MATLAB Signal Processing Toolbox. A polynomial can be fit to the PSD magnitudes and then subsequently differentiated to obtain the curvature values[5]. Interpolation procedures can generate additional d.o.f. at locations between sensors, which may increase the accuracy of locating damage between sensors. A cubic polynomial function was used to fit PSD data between the measuring points. Ten points were chosen to approximate the PSD magnitude between each pair of measured points. Consequently, the total distance between measuring points is divisible to 200 nodes, as shown in Fig. 3. Curvature values of PSD used in Eq. (5) depend on the interpolation function used to fit PSD data. Different interpolation schemes were used to fit the PSD and the obtained results were compared. The use of a cubic polynomial function and spline interpolation scheme to fit the PSD data yielded better results in detecting and locating damage than use of linear or nearest interpolation schemes. Different interpolation methods were applied using MATLAB standard[12].

3.2 Damage scenarios

The damage that was introduced was intended to simulate fatigue cracking, which has often been observed in plate-girder bridges. This type of cracking results from out-of-plane bending of the plate girder web. It usually begins at welded attachments to the web such as seats supporting the floor beams. Damage was introduced by making various torch cuts in the girder web and flange. The torch cuts produce simulated cracks that are too wide to open and close under the levels of excitation used in this investigation. Therefore, nonlinear effects associated with fatigue crack opening and closing cannot be studied in this investigation. In this study, damage was simulated by removing a triangular shell element in most damage cases, as shown in Fig. 4. This method of modeling the damage changes the geometry only. It introduces no nonlinearities into the model. Therefore, a linear modal analysis can be performed to ascertain effects of this damage on dynamic properties of the structure. The damage cases are:

Case I – removing a triangular shell element, 0.2 × 0.5 m, at node 33 (Fig. 3), at approximately the mid-height of the web (Fig. 4).
Case II – removing a triangular shell element, 0.2 × 0.5 m, at node 66 at approximately the mid-height of the web.
Case III – removing a triangular shell element, 0.2 × 0.5 m, at node 100 (center of the beam) at approximately the mid-height of the web.
Case IV – the same as Case I, but the crack position is moved in the vertical direction to the top of the web to be further from the position of the acceleration response measurement.
Case V – removing a triangular shell element, 0.2 × 0.5 m, at node 33 on the lower flange.
Case VI – removing a triangular shell element, 0.2 × 0.5 m, at two nodes, 66 and 116, at approximately the mid-height of the web.
Case VII – the same as Case I, but a different excitation force signal is used for the damaged structure.
Case VIII – the same as Case I, random excitation forces, simulating ambient vibration caused by traffic, are used for the intact structure. Different distribution and different magnitude of the forces are used for the damaged structure.
Case IX – the same as Case I, but instead of using the intact structure as a baseline for comparison, the bridge with slight damage (0.2 × 0.25 m) is taken as the intact case and the bridge with greater damage (0.2 × 0.5 m) is taken as the damaged case.
Case X – the same as Case I, but the distance between measuring points is increased from 3 m to 6 m.

4. Application of the proposed algorithm to different damage cases

4.1 Case I

Fig. 5 shows obtained results when the algorithm is applied for damage Case I (at node 33). The damage is detected at nodes 30 and 31 with a smaller indication of damage at 39 and 40. The accumulated

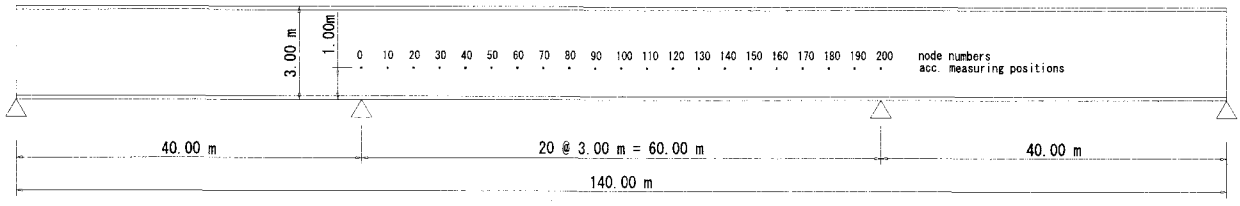

Fig. 3 Acceleration measurement positions at mid-span of the main girder and node numbers

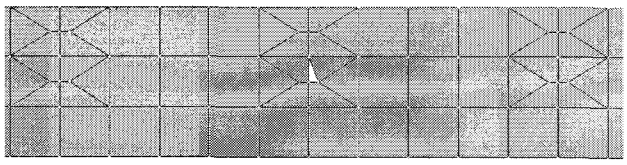

Fig. 4 Simulation of damage by removal of a triangular shell element

damage indicator values are very high at nodes 30 and 31, confirming the existence of damage at those nodes. The indication of damage at node 40 appeared because the actual position of damage exists between nodes 30 and 40 (where the acceleration response is measured). The authors infer that this level of accuracy in localizing the damage position in such big structures is satisfactory. The number of times of detecting the damage is determined using Eq. (13). Damage is detected 88 times at node 30 ($O_{30} = 88$), 85 times at node 31, 26 times at node 39 and 21 times at node 40, as shown in Fig. 6. It is noteworthy that no indication of damage appeared in any other position aside from the damaged zone. A PSD magnitude in the frequency range of 1–10 Hz was used in the proposed algorithm. In addition, the same frequency range was used in all damage cases except for Case VI. Fig. 7 shows the indicated position of damage versus the frequency value at which PSD is measured. Damage is detected accurately at almost all frequency values in that range.

4.2 Case II

The accuracy of damage identification methods based on mode shapes is sometimes reduced when the damage exists at the node of the used modes. Therefore, the damage position is changed in this case and Case III to examine the effects of changing the damage position. The obtained results of this case are shown in Figs. 8 and 9. The damage is indicated accurately at node 61; the accumulated damage indicator value decreased compared to its value for Case I (at node 33). It is noteworthy that damage is usually predicted at one of the nearest reading positions. Damage exists in this case at node 66 between reading positions at nodes 60 and 70. Therefore, it is detected at node 60.

4.3 Case III

This damage case is introduced to meet two objectives: we confirm the feasibility of the proposed algorithm to detect damage at different positions and examine the effect of locating damage at or very near the reading position. The damage is detected exactly around node 100, as shown in Figs 10 and 11. Therefore, we conclude that

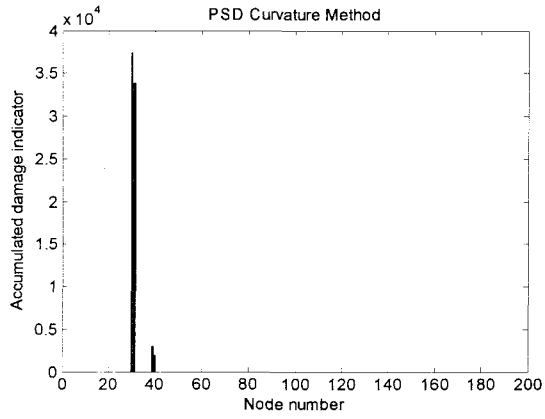

Fig. 5 Proposed algorithm applied to damage Case I

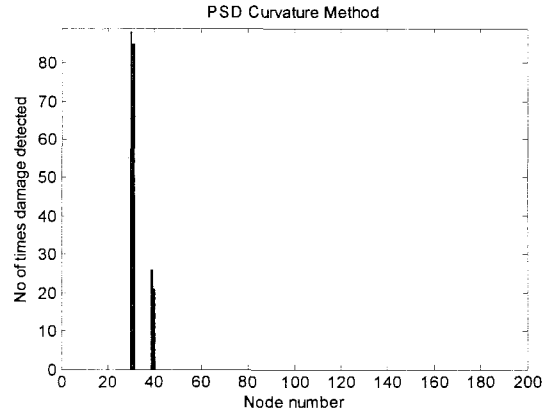

Fig. 6 Number of times of detecting damage for Case I

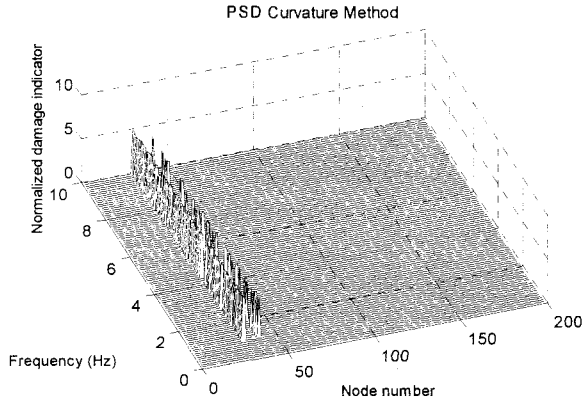

Fig. 7 Predicted position of damage vs. frequency for Case I

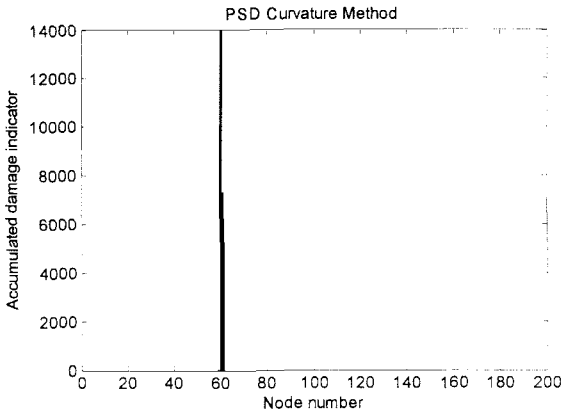

Fig. 8 Proposed algorithm applied to damage Case II

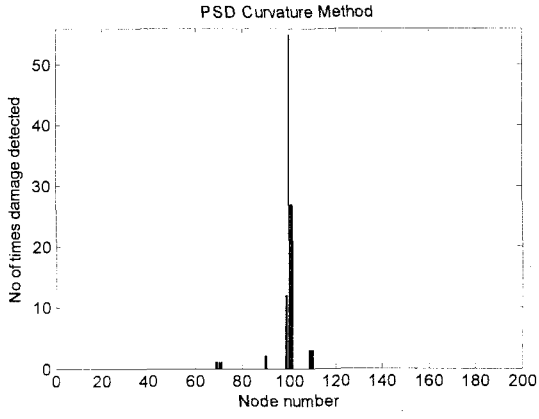

Fig. 11 Number of times of detecting damage for Case III

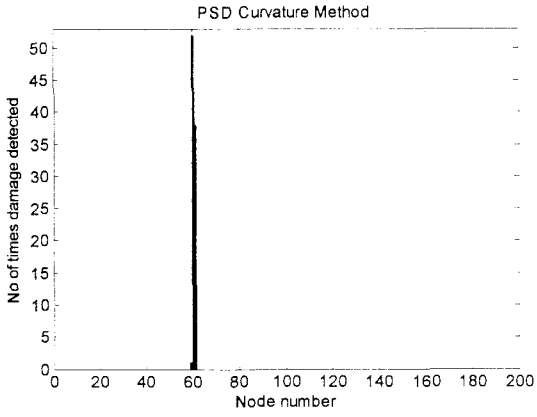

Fig. 9 Number of times of detecting damage for Case II

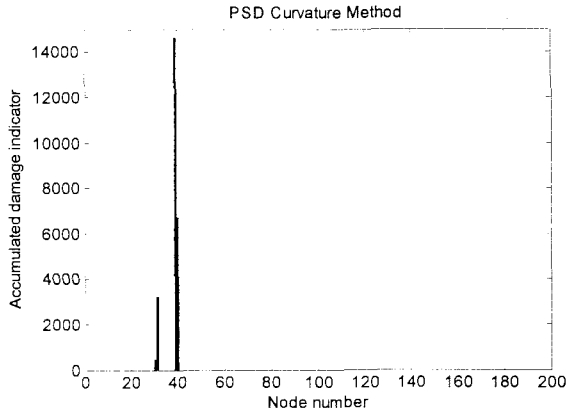

Fig. 12 Proposed algorithm applied to damage Case IV

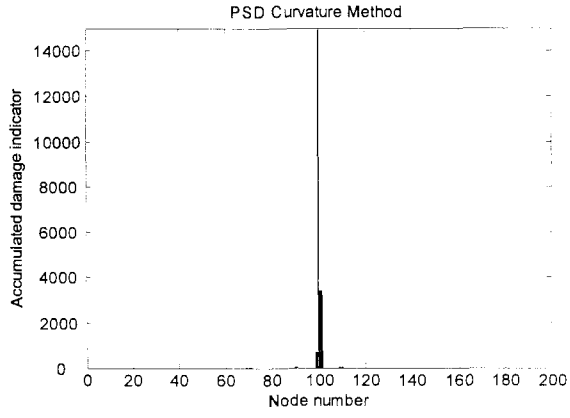

Fig. 10 Proposed algorithm applied to damage Case III

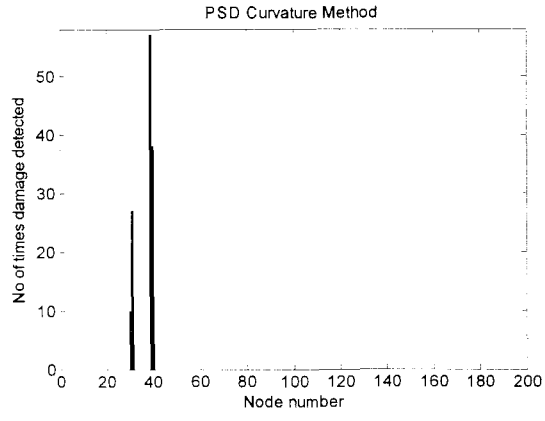

Fig. 13 Number of times of detecting damage for Case IV

damage near the reading positions (sensors) is located more accurately than damage between the reading positions.

4.4 Case IV

Effects of changing the damage position in the horizontal direction (parallel to the measuring points) were examined in previous cases of damage. In this case, damage at node 33 (Case I) is moved in the vertical direction to the top of the web (about 2 m above the measuring line). As indicated clearly in Figs. 12 and 13, the damage is detected accurately between nodes 30 and 40 with smaller values of accumulated damage indicator and fewer number of times of detecting the damage than in Case I.

4.5 Case V

In this case, damage is introduced to the lower flange of the main girder. The acceleration response of the bridge, as explained before, is measured along one line on the web of the main girder. Although flange damage is expected to reduce the overall stiffness of the main girder, it is more difficult to predict using the acceleration response of the web. When the proposed algorithm is applied to this case, the

position of damage is predicted between nodes 20 and 30 with a high accumulated damage indicator, as shown in Fig. 14. The actual position of damage exists between nodes 30 and 40. Therefore, the indicated position at node 30 is accurate, whereas the indicated position at node 20 is a false positive reading. This false positive reading is near the actual damage position. Again, this accuracy is considered satisfactory for large structures.

4.6 Case VI

This case is introduced to investigate the feasibility of the algorithm to detect multiple-damage. The PSD magnitude is measured in the frequency range of 1–5 Hz. Damage at the two positions is detected and localized accurately with no false positive readings, as shown in Fig. 15. As indicated in this figure, damage at node 66 is predicted at nodes 60 and 70 and damage at node 116 is predicted at node 120. The accumulated damage indicator value at node 60 is higher than that at node 120. When the PSD was measured in the frequency range of 1–10 Hz, the damage indicator value at node 60 was much higher than its value at node 120 in a way that reduced the appearance of the bar at node 120. For that reason, it is recommended that the results of the normalized damage indicator versus frequency (Fig. 16) be shown to confirm the predicted results at each damage location.

4.7 Case VII

In this case, the random signal used for the excitation force differs for intact and damaged structures. The excitation force is applied at the bridge deck center in both cases. Acceleration responses near the center of the main girder for intact and damaged structures are shown respectively in Figs. 17 and 18. Although damage at node 33 was detected accurately as shown in Fig. 19, the accumulated damage indicator value decreased markedly compared to Case I of damage (Fig. 5) where the same excitation force is used for both intact and damaged structures.

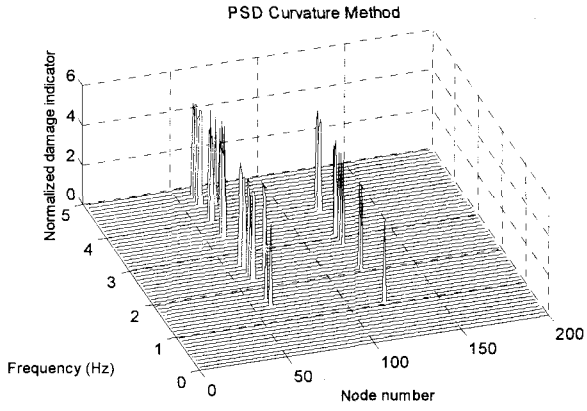

Fig. 16 Predicted position of damage vs. frequency for Case VI

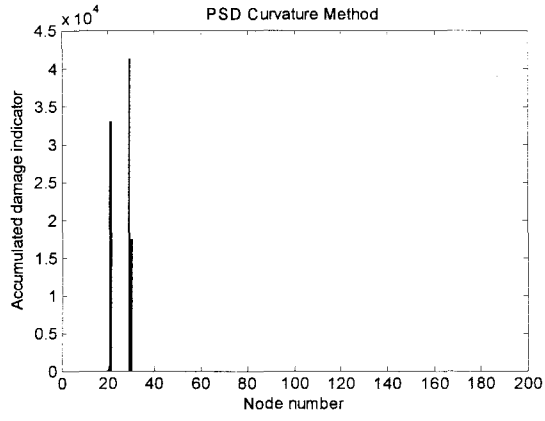

Fig. 14 Proposed algorithm applied to damage Case V

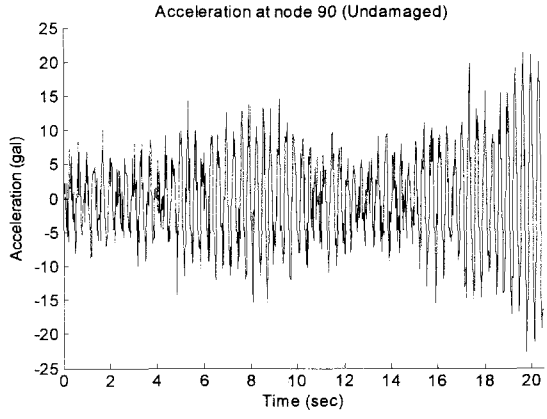

Fig. 17 Acceleration response of the intact structure at node 90

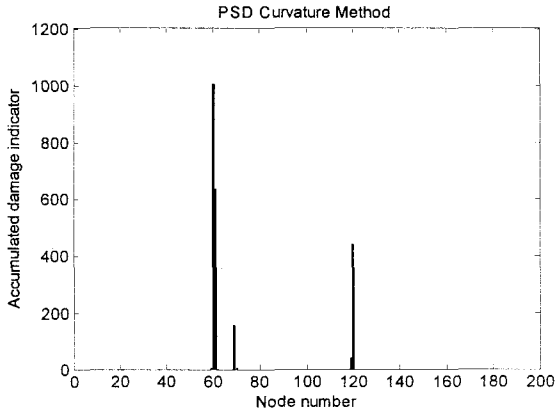

Fig. 15 Proposed algorithm applied to damage Case VI

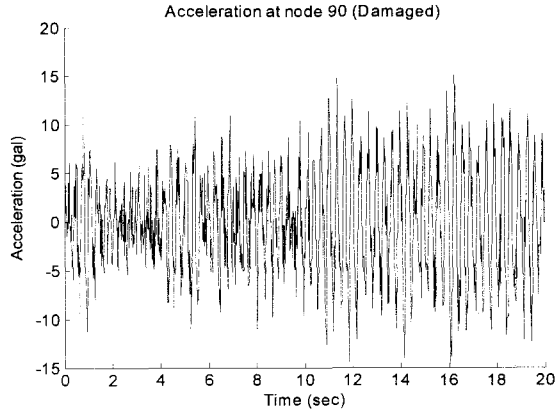

Fig. 18 Acceleration response of the damaged structure at node 90

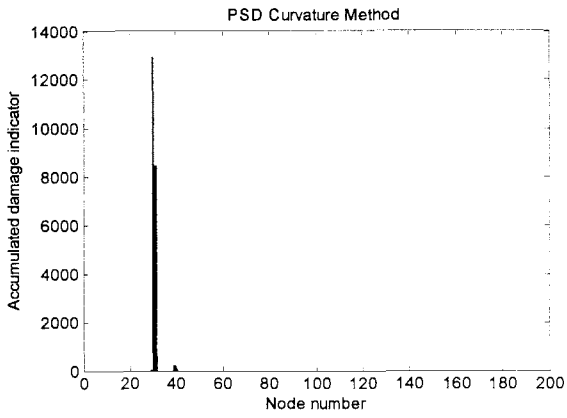

Fig. 19 Proposed algorithm applied to damage Case VII

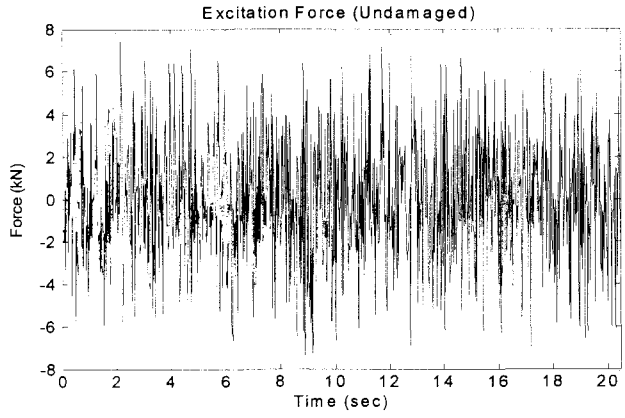

Fig. 20 Excitation force used for the intact structure for Case VIII

4.8 Case VIII

A future goal of a comprehensive bridge management system is to have a self-monitoring bridge for which sensors feed measured responses (accelerations, strains, etc.) into a local computer. This computer would, in turn, apply a damage identification algorithm to this data to determine if the bridge integrity has deteriorated enough to jeopardize user safety. The local computer in an actual system would then contact a central monitoring facility to notify maintenance or safety officials of the bridge's condition[5]. If such a monitoring system is ever to be practical, it must predict structural damage using ambient, traffic-induced vibration. To this end, all damage results that have been identified by the proposed algorithm were determined without using measured input to the structure.

For this purpose, instead of using one concentrated load that simulates the shaker force, different loads are distributed randomly on the concrete deck to simulate a random distribution of cars passing over the bridge. Different random time history signals with different peak amplitudes are used for the intact and damaged structures. The random time history signals used for the intact and damaged structures are shown respectively in Figs. 20 and 21. Excitation forces are applied as time-variant concentrated vertical loads distributed on the bridge deck. Damage at node 33 is detected and located accurately, as shown in Fig. 22. However, the accumulated damage indicator values are very low and the number of times of detecting the damage is also lower (Fig. 23) than for Case I of damage, in which the same excitation force was used at the same position for the intact and damaged structures. Therefore, using a shaker force with the same signal, the same peak amplitude and applied at the same position for the intact and damaged structures will yield the most accurate and definitive results using the proposed algorithm.

4.9 Case IX

The above analysis presumes that the baseline for comparison is the intact case. To consider the extension of damage from a damaged bridge to another severe damaged one, changes in the curvature of PSD magnitude for the test structure are investigated. Fig. 24 shows the change in PSD curvature between the damaged bridge with crack sizes of 0.20 × 0.25 m and 0.20 × 0.50 m. This figure reflects PSD

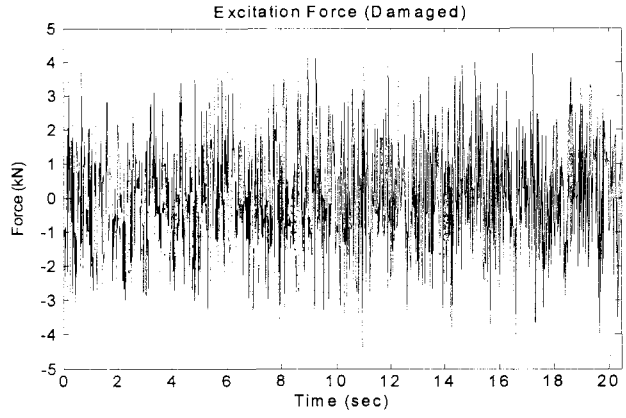

Fig. 21 Excitation force used for the damaged structure for Case VIII

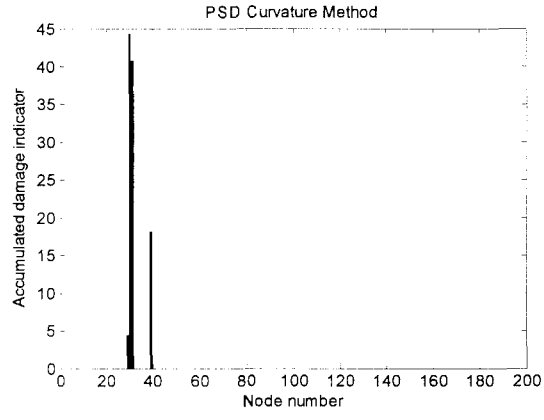

Fig. 22 Proposed algorithm applied to damage Case VIII

localization for damage extension, considering the less damaged bridge as the baseline case. The above results indicate that changes in the curvature of PSD magnitude are effective and robust for detecting and locating both the initiation and extension of damage in a structure. Indeed, the convenience of using changes in PSD curvature is that they are localized at the damaged region and are applicable using only the lower range of frequency, which is easily measurable.

4.10 Case X

In the previous analysis, the acceleration response was measured

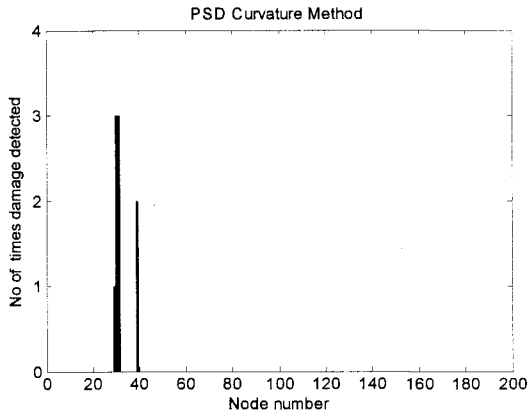

Fig. 23 Number of times of detecting damage for Case VIII

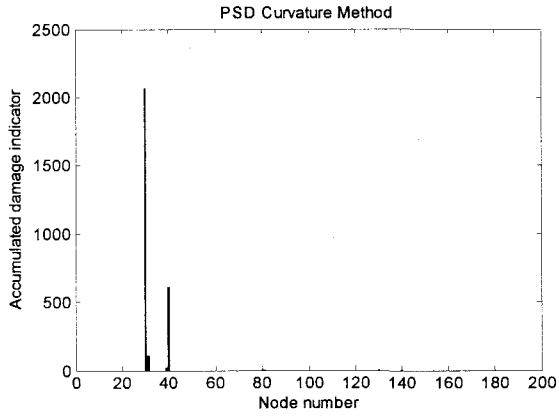

Fig. 24 Proposed algorithm applied to damage Case IX

along one line and the distance between the measuring points was 3 m. Nevertheless, in actual practice, fewer sensors are typically desired because of their high cost. Therefore, reduced sets of data were used to determine how the results change using coarser measurement grids. The step of measurements is increased from 3 m to 6 m, i.e., the measurements are reduced by approximately one-half. In this case, measuring points are located at nodes 0, 20, 40, 60, …, and 200. A cubic polynomial function is also used to approximate PSD data between the measuring points. We chose 20 readings between each pair of measuring points to produce an equal number of nodes to the previous cases. Figs. 25 and 26 respectively show the accumulated damage indicator and the number of time of detecting the damage at node 33 using the frequency range of 1–10 Hz. Damage is detected clearly with a very high-accumulated damage indicator value. Furthermore, the number of damage instances detected is also high as compared to the case of using a fine grid of measurements; no false positive readings were obtained. On the other hand, the damage is detected between the nearest measuring points, as noted in the previous cases, implying lower damage-position locational accuracy. Therefore, we infer that decreasing the number of sensors did not affect the accuracy of detecting the damage, but reduced the accuracy of locating the damage position.

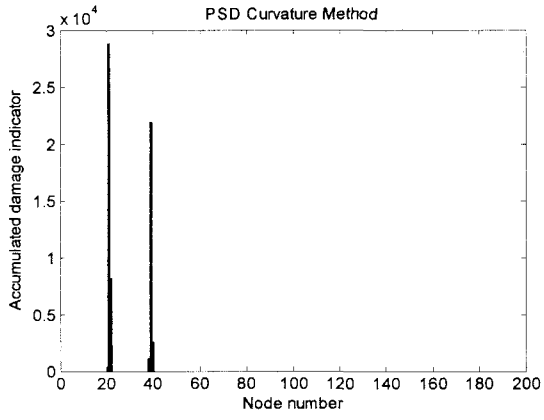

Fig. 25 Proposed algorithm applied to damage Case X

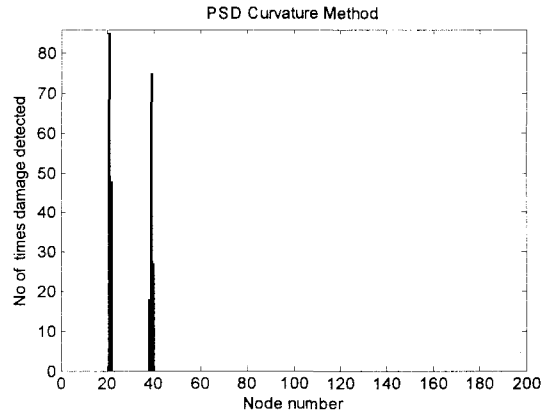

Fig. 26 Number of times of detecting damage for Case X

4.11 The effect of PSD normalization

The PSD data must be normalized, as explained previously, because the PSD magnitude depends on the excitation force amplitude. Therefore, if the excitation force used for the intact structure differs from that used for the damaged structure, the PSD must be normalized. On the other hand, normalization of the PSD changes PSD data from its original state because the data are divided by different factors depending on the original PSD values. These changes or approximations in PSD data because of normalization are small and the accuracy of the results is usually acceptable. When using the same excitation force (same signal and same amplitude) at the same position for both intact and damaged structures, the PSD can be used without normalization. In this case, PSD data include no approximations: changes in the PSD curvature result only from damage. A new case of damage is introduced to elucidate the effect of using PSD without normalization. In Case I, explained previously, instead of removing a triangular shell element to simulate crack at node 33, the cross sectional area of this triangular shell element is decreased by 50% to simulate reduction in the cross sectional area because of rust. This case of damage represents the smallest damage introduced in this study. Figs. 27 and 28 show obtained results when the PSD is normalized and not normalized, respectively. Results obtained from the two techniques showed the following:

1- Damage was detected at nodes 30 and 40 in case of using normalized PSD; it was detected more accurately at node 30

only when using non-normalized PSD.

2- False positive readings appeared at nodes 60, 110 and 120 when normalized PSD was used. On the other hand, no false positive readings occurred when non-normalized PSD was used.

3- The accumulated damage indicator value at the damage position is much higher when using non-normalized PSD than when using normalized PSD.

4- Damage around node 30 was detected 70 times when non-normalized PSD was used and 15 times when normalized PSD was used.

When non-normalized PSD was used for all the previous damage cases, results that are more accurate were obtained except for Cases VIII and IX, in which the excitation forces used for the intact and damaged structures were different. Therefore, in the case of using shaker force for excitation, PSD can be used without normalization. When using ambient vibration as an excitation force, PSD must be normalized.

5. Application of the change in CSD method to some damage cases

In this section, the change in CSD method is applied to some damage cases to compare results of this method and the PSD curvature method. The CSDs are calculated for the measured acceleration between one reference channel and different measuring points. The reference channel was chosen between nodes 100 and 110 (Fig. 3); it is located 2 m from node 100 and 1 m from node 110. The frequency range used for measuring CSD for different cases of damage is the same as the range used for the PSD curvature method. The same window size and sampling rate are used for both methods.

5.1 Cases I, II and III

Fig. 29 shows results of the change in CSD method for Case I. Damage at node 33 is detected accurately at nodes 30 and 31 with no false positive readings. The damage at nodes 30 and 31 is detected 73 times, as determined from Eq. (20). Comparing the results obtained from this method to the results of PSD curvature method (Fig. 5), we conclude that both methods detected the damage accurately. In addition, damage indicator values for the PSD curvature method around the position of damage are much higher than the values for the change in CSD method. Moreover, the number of times of detecting the damage around the correct position of damage, as determined by PSD method (173) is greater than that determined by CSD method (73). When CSD method was applied to Cases II and III, similar results to Case I were observed. The CSD method detects the damage accurately with lower values of accumulated damage indicators and fewer times of damage detection. Some false positive readings appeared in Case II and Case III.

5.2 Case IV

When the damage location became far from the acceleration reading positions (sensor positions), the accuracy of change in CSD

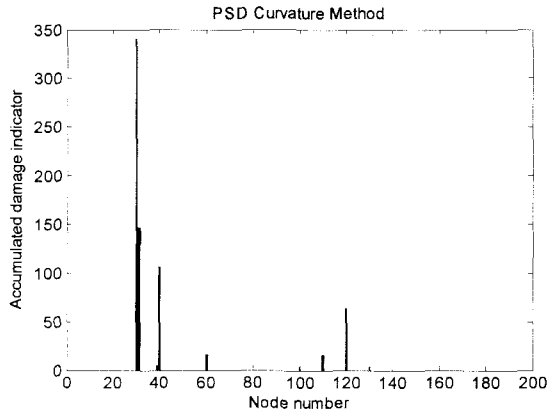

Fig. 27 Proposed algorithm applied for 50% damage at node 33 using normalized PSD

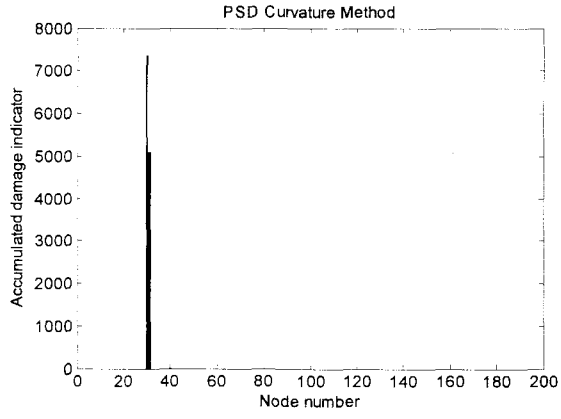

Fig. 28 Proposed algorithm applied for 50% damage at node 33 using non-normalized PSD

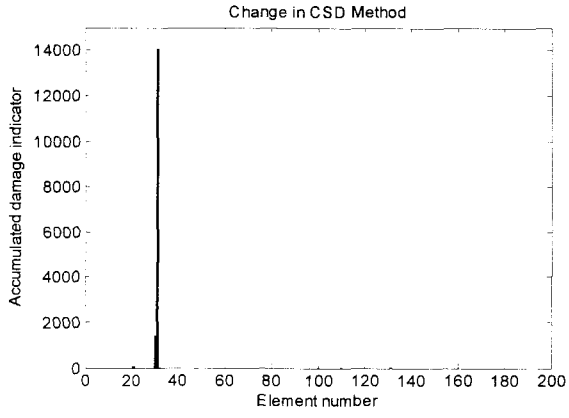

Fig. 29 Change in CSD method applied to damage Case I

method decreased. Several false positive readings appeared, as shown in Fig. 30. PSD method showed better results for this damage case (Fig. 12).

5.3 Case VI

For the case of multiple-damage, CSD method detected the damage at node 66 accurately. On the other hand, damage at node 116 is detected at three locations as shown in Fig. 31: 110, 120 and

130. For this case, PSD method performed better than CSD method.

5.4 Case IX

When CSD was applied to detect the increase of damage at node 33, a large number of false positive readings appeared at different locations, which degraded the indicated position of the correct damage location, as shown in Fig. 32.

5.5 Comparing results of damage identification methods

Table (1) summarizes the results obtained from the two methods for different damage cases. The table shows the accumulated damage indicator value, the number of times of damage detection, and the number of locations of false positive readings determined by each damage identification method for each damage case. All cases of damage showed that the PSD curvature method detected the damage with a higher value of accumulated damage indicator except for Case X, a higher number of times of damage detection, except for Case III and a lower number of false-positive locations. Therefore, we conclude that the PSD curvature method is more sensitive for damage detecting than the CSD method.

Table (1) Comparison of the results of damage identification methods

Dmg. Case	Acc. Dmg. Indicator Value		No. of times of detecting damage		No. of locations of false positive readings	
	PSD	CSD	PSD	CSD	PSD	CSD
I	3.74 E4	1.41 E4	173	73	0	0
II	1.40 E4	7583	91	63	0	5
III	1.49 E4	1.02 E4	94	115	0	7
IV	1.46 E4	163.5	95	7	0	5
V	4.13 E4	3.12 E4	153	139	1	1
VI	1004.1, 439.8	119.7, 37.6	28, 13	9, 6	0, 0	0, 1
VII	1.29 E4	5069.5	95	42	0	0
VIII	44.2	21.0	7	4	0	0
IX	2063.9	280.6	27	8	0	3
X	2.89 E4	4.15 E4	133	227	0	0

6. Concluding remarks

(1) We investigated changes in the curvature of PSD magnitude that are attributable to the presence of structural damage, as represented in this numerical finite element model. Results for this steel bridge model demonstrate the usefulness of changes in the curvature of PSD magnitude as a diagnostic parameter for detecting and locating damage in the main girder of the steel bridge with different damage cases.

(2) The proposed algorithm showed good results for detecting and locating damage in different places and for single and multiple-damage cases. Moreover, the use of changes in the curvature of PSD magnitude is effective and robust in detecting and locating both the initiation and extension of damage throughout a structure.

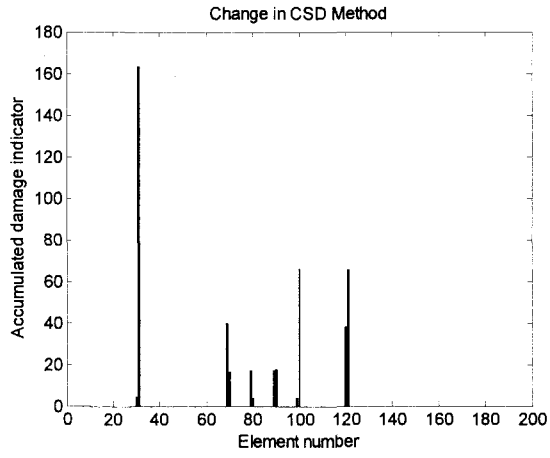

Fig. 30 Change in CSD method applied to damage Case IV

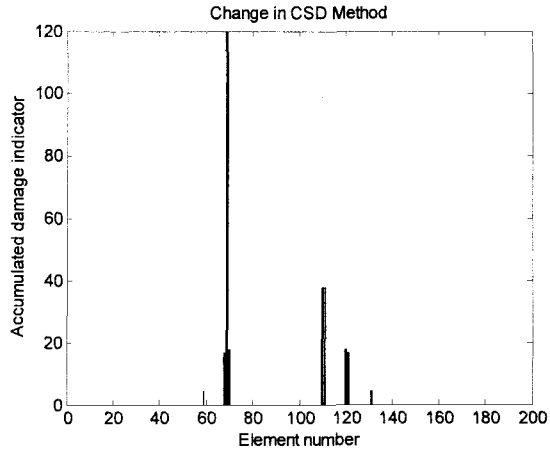

Fig. 31 Change in CSD method applied to damage Case VI

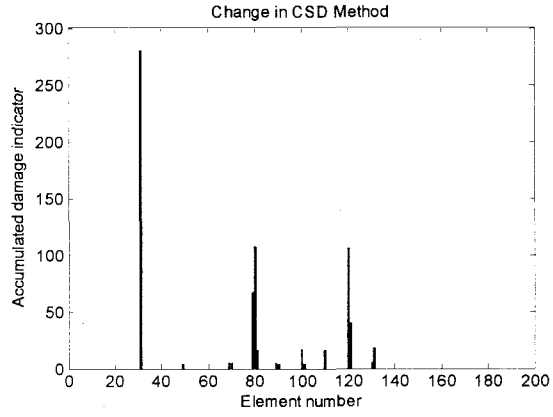

Fig. 32 Change in CSD method applied to damage Case IX

(3) All damage results that were identified by the proposed algorithm were determined without using the measured input to the structure because PSD is measured from the structure's acceleration response. Therefore, the algorithm can be a useful tool for continuous health monitoring of structures using ambient vibration as an excitation force. On the other hand, when different excitation forces (different distribution, different excitation signal and different force peak amplitude) are used for intact and damaged structures, the damage is

detected and localized less accurately than in the case of using the same excitation force for exciting both the intact and damaged structures.

(4) Damage was detected and located accurately in most damage cases presented here using a low range of frequency without any need for measuring modal data or higher modes.

(5) Damage was located more accurately when it occurred very near a measuring point. On the other hand, when damage occurs between the measuring points, the damage is located, or sensed, at a nearby measuring point. Therefore, we noted that reducing the number of sensors did not affect the accuracy of detecting the damage, but reduced the accuracy of locating the damage position. If the damage position could be detected within the distance between sensors, then another localized damage detection method such as ultrasonic or visual inspection should be applied to the suspected area.

(6) When using the same excitation force for intact and damaged structures, using non-normalized PSD data in the proposed algorithm exhibited more accurate results in detecting and locating damage than using normalized PSD data. However, PSD must be normalized when using ambient vibration data or different excitation forces for intact and damaged structures.

(7) PSD curvature method yielded better results in detecting and locating damage than change in CSD method, especially for the case in which the damage was located far from the reading positions, the case of measuring the extension of damage and in case of multiple-damage.

References

1) Kim J. - T., and Stubbs N., Crack Detection in Beam-Type Structures Using Frequency Data, *Journal of Sound and Vibration*, 259(1), 145–160, Williamsburg, VA, 2003.

2) Park, S., Stubbs, N. and Bolton, R.W., Damage Detection on a Steel Frame Using Simulated Modal Data, *16th International Modal Analysis Conference (IMAC XVI)*, Santa Barbara, California, February 2-5, Proceedings, pp. 612–622, 1998.

3) Abdo M. A.-B. and Hori M., A Numerical Study of Structural Damage Detection Using Changes In The Rotation of Mode Shapes, *Journal of Sound and Vibration*, 251(2), pp. 227-239, 2002.

4) Ewins D. J., *Modal Testing: Theory and Practice*, John Wiley, New York, 1985.

5) Farrar C. R. and D. A. Jauregui, *Damage Detection Algorithms Applied to Experimental and Numerical Model Data from the I-40 Bridge*, Los Alamos National Laboratory Report, LA-12979-MS, 1996.

6) Oshima T. et al., Study on damage evaluation of joint in steel member by using local vibration excitation, (In Japanese), *Journal of Applied Mechanics JSCE*, Vol.5, pp.837-846, 2002.

7) Beskhyroun S., Oshima T. et al., Damage detection and localization on structural connections using vibration based damage identification methods, *Journal of Applied Mechanics, JSCE*, Vol.6, pp. 1055-1064, 2003.

8) McLamore, V. R., G. C. Hart and L. R. Stubbs, Ambient Vibration of Two Suspension Bridges, *Proceedings of the ASCE Journal of the Structural Division*, 97, 2567-2582. 1971.

9) Farrar C. R. et al., *Dynamic Characterization and Damage Detection in the I-40 Bridge Over the Rio Grande*, A Literature Review, Los Alamos National Laboratory Report, LA-12767-MS, 1994.

10) Beskhyroun S., Mikami S., Oshima T. and Yamazaki T., Modified damage identification algorithm based on vibration measurements, *Journal of Applied Mechanics, JSCE*, Vol.7, pp. 97-107, 2004.

11) SAP2000, *Integrated Finite Element and Design of Structures*, Analysis Reference Manual, Computers and Structures, Inc. Berkeley, CA, USA, 1995.

12) MATLAB Reference Guide, The Math Works, Inc., Natick, MA, 1992.

13) MATLAB User's Guide, The Math Works, Inc., Natick, MA, 1992.

(Received: September 17, 2004)